ACS NANO

ARTICLE

Conformable Nanowire-in-Nanofiber Hybrids for Low-Threshold Optical Gain in the Ultraviolet

Alberto Portone, Rocio Borrego-Varillas, Lucia Ganzer, Riccardo Di Corato, Antonio Qualtieri, Luana Persano, Andrea Camposeo, Giulio Cerullo,* and Dario Pisignano*

Cite This: *ACS Nano* 2020, 14, 8093−8102

Read Online

ACCESS | Metrics & More | Article Recommendations | SI Supporting Information

ABSTRACT: The miniaturization of diagnostic devices that exploit optical detection schemes requires the design of light sources combining small size, high performance for effective excitation of chromophores, and mechanical flexibility for easy coupling to components with complex and nonplanar shapes. Here, ZnO nanowire-in-fiber hybrids with internal architectural order are introduced, exhibiting a combination of polarized stimulated emission, low propagation losses of light modes, and structural flexibility. Ultrafast transient absorption experiments on the electrospun material show optical gain which gives rise to amplified spontaneous emission with a threshold lower than the value found in films. These systems are highly flexible and can conveniently conform to curved surfaces, which makes them appealing active elements for various device platforms, such as bendable lasers, optical networks, and sensors, as well as for application in bioimaging, photo-cross-linking, and optogenetics.

KEYWORDS: organic−inorganic materials, nanocomposites, zinc oxide, electrospinning, amplified spontaneous emission, ultrafast transient absorption
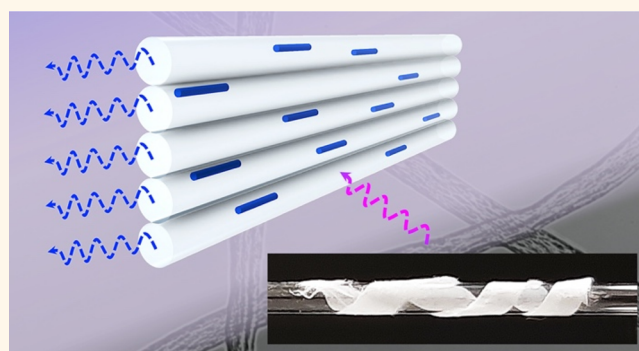
The development of miniaturized and effective light sources with emission in the near-ultraviolet (UV) is highly important for all those fields, including microanalysis through fluorescence spectroscopy, chemical sensing, and healthcare diagnostics, where molecular photo-excitation is involved.[1−4] Together with mechanical flexibility to have them conformed to different surfaces or lodged within different lab-on-chip platforms,[2,3,5,6] UV-active materials are desired to feature stimulated emission and optical gain, which is the basic prerequisite to use them in compact laser systems and photonic networks. Examples of UV-emitters include various inorganics (GaN, ZnS, ZnO, *etc.*) and their nanostructures grown through chemical vapor transport processes, colloidal synthesis, and other deposition methods.[7−12] Inorganic nanostructures, and especially nanowires (NWs), have been largely exploited within semiconductor-embedding optical cavities, plasmonic nanolasers, and heterojunctions.[7,9,12,13] However, the so-obtained devices are largely limited to planar systems or substrates for nanostructure growth, and they are mechanically stiff and unconformable to curved surfaces. Polymeric light-emitting materials and films,[3,14−17] instead, can be easily coupled with bendable substrates and are more versatile in terms of configurational motifs, although their optical performance and stimulated emission properties are generally much less appealing and stable in time compared to inorganics.

Hybrid approaches, inserting highly efficient and stable oxide nanosystems in flexible polymer nanostructures and enabling high-throughput processing, would combine advantages of UV light-emitting inorganics and plastic matrices and potentially lead to materials with enhanced properties. For instance, in these systems, light from UV nanoscale emitters could be efficiently coupled to polymer waveguides and transported along macroscale distances,[3,18] thus overcoming the high propagation losses typical of individual inorganic nanostructures[19] and enabling a much more versatile device
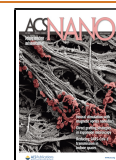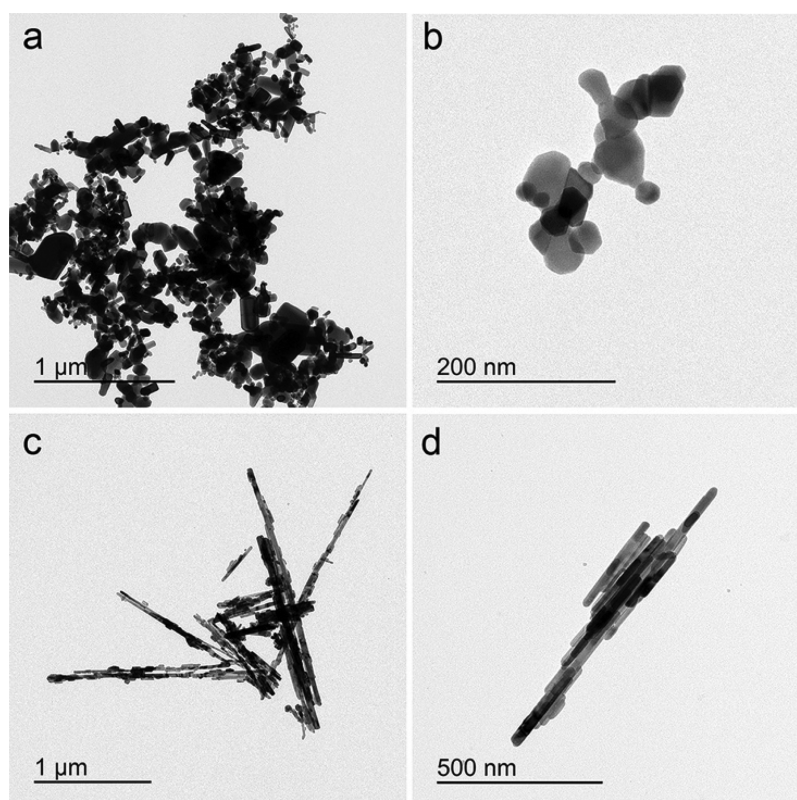
Figure 1. TEM images of used ZnO NPs (a,b) and ZnO NWs (c,d) at different magnifications. Both NPs and NWs easily form clusters before imaging.

interfacing. A few attempts at fabricating luminescent poly-(ethylene terephthalate) or poly(vinyl alcohol) nanofibers embedding ZnO or Ge nanocrystals have been reported,[20,21] nonetheless the stimulated emission and optical gain properties of hybrid functional materials in the UV spectral range are still unexplored. In this work, we introduce hybrids encompassing UV-emitting ZnO NWs in polymer fibers and report on their optical gain properties. ZnO thin films and nanostructures are highly interesting due to their large exciton binding energy (∼60 meV), efficient radiative recombination at room temperature, and large band gap (∼3.3 eV), which provides very stable and narrow luminescence between 370 and 390 nm[7,22−24] and even a potential for reliable polariton lasing at room temperature following embedding in microcavities.[25] In fact, previous methods based on *in situ* synthesis of ZnO nanocrystals from zinc acetate dehydrate precursors[20] have led to isotropic nanoparticles (NPs) or grain aggregates in fibers, which are hard to engineer in order to obtain NWs in hybrids without increased surface roughness, that are instead desired to promote light transport and amplification. Here, the incorporation of ZnO NWs in transparent[3] poly(methyl methacrylate) (PMMA) electrospun filaments leads to a NW-in-fiber hybrid material with internal architectural order, combining optical gain, polarized stimulated emission, and waveguiding properties in an efficient system for flexible UV lasers operating at room temperature. The internal alignment of NWs promoted by electrospinning is found to be critically relevant in making ZnO NW-in-fiber hybrids capable of outperforming counterparts doped by non-elongated ZnO NPs, in terms of reduced optical losses as well as low amplified spontaneous emission (ASE) threshold.

The relevance of the here reported results is two-fold, that is, at both fundamental and practical levels. Ultrafast transient absorption measurements with high temporal resolution (20 fs) are presented for the ZnO NW-in-fiber hybrids. These measurements provide insight into the ultrafast non-equilibrium physics of ZnO NWs in the hybrid material, enabling the observation of carrier scattering with optical phonons and of a shift in absorption due to photogenerated charges (Burstein−Moss effect), thus providing insight into the ultrafast non-equilibrium physics of ZnO NWs in the hybrid material. In addition, these hybrids can lead to the definition of design rules for miniaturized lasers, bio- and chemical sensors, and optical networks embedding UV-emitting materials and nanocomponents. Indeed, the optical gain in the hybrid system incorporating elongated NPs can benefit from having them aligned in electrospun polymers,[26] promoting enhanced forward scattering,[27,28] and channeling photons along the longitudinal axis of the fibers. The latest applications benefiting from the advanced combination of properties of NW-in-fibers include wearable components for healthcare monitoring and biometric recognition and devices for optogenetics, photochemical cross-linking of proteins, localized calcium imaging, and immunological modulation.[29−32]

RESULTS AND DISCUSSION

The used ZnO nanomaterials, including nonelongated NPs and NWs, are initially inspected by transmission electron microscopy (TEM, Figure 1). NPs generally exhibit diameters below 100 nm, whereas NWs have a transverse section of about (40 ± 15) nm and various lengths with a maximum on the order of 1 μm, leading to an aspect ratio (length/diameter) below 25. For NWs with this transversal size and length, one
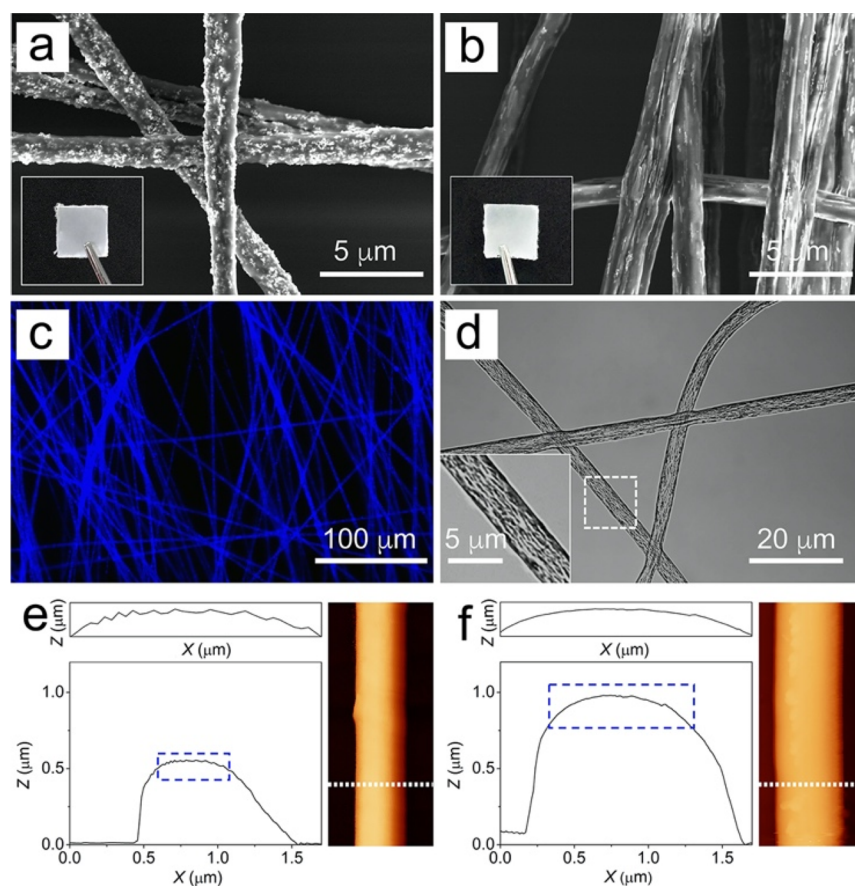
Figure 2. (a,b) SEM micrographs of fibers doped with ZnO NPs (a) and ZnO NWs (b). Insets show the photographs of the fibrous samples. (c) A fluorescence image of electrospun fibers doped with ZnO NPs. (d) ZnO NWs-doped fibers imaged by transmitted light microscopy. Inset: Magnification of the sample area highlighted by a dashed square box. (e,f) Profiles of exemplary fibers incorporating ZnO NPs (e) and ZnO NWs (f), along the dashed line in the corresponding AFM images shown on the right of the graphs. Top panels: Magnifications of the profile regions in the blue-dashed rectangles (top regions of fibers). Relative weight ratio (NPs/polymer or NWs/polymer) in the electrospinning solution: χ = 30%.

could expect a minor influence of surface effects on optical properties.[33,34] In addition, for this range of sizes, quantum confinement effects do not play a significant role, and the electronic and optical properties of the nanomaterials resemble those of the bulk.[35,36] The dispersion in size of ZnO NPs and NWs is not found to affect significantly the fabrication process of doped fibers. In fact, in order to embed these systems in polymer filaments with limited aggregation and precipitation, dispersions of NPs and NWs are prepared with a mixture of chloroform and ethanol (1:1 v:v) following extensive solubility tests (see Figure S1 in the Supporting Information file). Dimethylformamide (DMF) is also added to reduce the overall solvent evaporation rate and avoid needle clogging during electrospinning.

Exemplary scanning electron microscopy (SEM) images of ZnO NPs- and NWs-doped fibers, spun from solutions with nanomaterial/polymer ratio (χ) as high as 30% in weight, are shown in Figure 2a,b. The corresponding diameter distributions, for fibers with different doping, are displayed in Figure S2. The average diameter of the fibers is found to slightly increase upon increasing χ, up to a maximum of about 1.8 μm, which is associated with the varied rheology of the electrospun solution.[37] Fibers are fluorescent, and the uniform emission signal collected from different segments of each filament (Figure 2c) as well as TEM imaging (Figure S3) indicate that

dopants are evenly distributed along the length of the filaments. Overall, fiber diameters are well above the cutoff value[38] (d_{cutoff}) for waveguiding at their emission wavelength ($d_{cutoff} \cong$ 160 nm, as estimated in Figures S4 and S5), which allows the intensity of the guided light modes to be effectively confined.

In addition, the SEM analysis strongly suggests a largely uniaxial alignment of NWs along the fiber length, which is also supported by optical transmission micrographs (Figure 2d). This alignment also involves NWs close to the fiber surfaces, thus significantly affecting external roughness of NW-in-fiber samples. Indeed, the surface of NW-in-fibers is significantly smoother (with root mean squared roughness, R_{q_NWs} = 19.7 nm) compared to that of NPs-doped fibers (R_{q_NPs} = 43.2 nm) where clustered particles may partially protrude out from the polymer surface, as measured by atomic force microscopy (AFM, Figure 2e,f). The alignment of ZnO NWs along the fiber longitudinal axis is also supported by TEM measurements on the hybrid filaments (Figure 3a,b) as well as by SEM performed by utilizing backscattered electrons (Figure 3c). The maximum misalignment angle is found to be as low as 10° (Figure 3d). Such a tight control of the NWs orientation is obtained during fiber generation and alignment promoted by the dynamics of elongated particles within the initially sink-like flow at the onset of the electrospinning process as well as
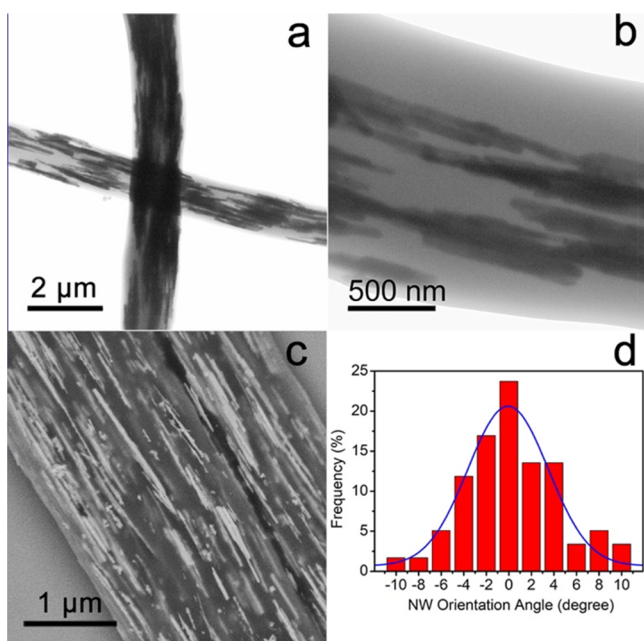
Figure 3. TEM (a,b) and SEM (c) micrographs of composite fibers with ZnO NWs. χ = 30%. (d) Distribution of the orientation angles of the ZnO NWs with respect to the fiber longitudinal axis. 0° corresponds to the direction parallel to fiber length.

within the stretching and thinning electrified solution.[26,39] Internal ordering of NWs within each polymer filament impacts on ASE properties, enhancing them as better detailed in the following. Indeed, the alignment of NWs is expected to minimize the propagation losses for radiation guided along the longitudinal axis of the hybrid fibers, because of the dominant forward component[27,28] of light-scattering at the ZnO/polymer interface (Figure S6), thus promoting waveguiding.

Reference absorption measurements performed on the hybrid materials highlight the typical features of ZnO,[40] with a single narrow peak at 374 nm due to the excitonic transition superimposed to a light-scattering background (Figure 4a). Photoluminescence (PL) properties are also analyzed on both spin-cast films and mats of fibers doped with either NPs or NWs, as displayed in Figure 4b,c. A bright UV emission band is measured, as typical of exciton recombination in ZnO, which peaks at 383 and 384 nm for NPs and NWs, respectively. Here, the spontaneous emission of the hybrid fibers (red lines in Figure 4b,c) is largely analogous to that of the corresponding films (black lines), with only minor red-shifts (1−3 nm) of the

peak wavelengths. This effect can be attributed to the slightly enhanced self-absorption, that is likely to be more effective in fibers due to their waveguiding properties, since these favor interactions of photoemitted light with embedded active NPs/NWs over longer effective distances. The insets of Figure 4b,c show a magnification of the emission spectra in the region between 450 and 700 nm. Here, a weak fluorescence is measured (1−2 orders of magnitude below the intensity of the main emission band in the UV), generally associated with ZnO surface states and defects such as oxygen and zinc vacancies and interstitials.[41−43] Furthermore, the comparison of the PL and ASE intensity from fibers electrospun from solutions with different NW/polymer ratios, measured under identical excitation and collection configurations, shows a brighter UV emission for χ = 30% (Figure S7). A lower PL intensity is measured for fibers obtained from χ = 50% solutions, which is likely related to higher self-absorption of the emitted light as also evidenced by the corresponding red-shift of the emission peak (Figure S7a). ASE is found only in fibers from χ = 30% solutions, with other hybrids suffering from either low content of the active medium (χ = 10%) or higher self-absorption (χ = 50%, Figure S7b).

In order to study the non-equilibrium optical response of the UV hybrid materials, we perform femtosecond pump−probe spectroscopy with excitation at 335 nm (3.7 eV) and broadband detection spanning from 330 to 550 nm. A 20 fs pump pulse is used to photoexcite carriers well above the bandgap of ZnO, whereas a delayed white-light-continuum probe pulse measures the differential transmission ($\Delta T/T$) spectrum as a function of time delay (see Methods). Figure 5a shows the $\Delta T/T$ map, as a function of probe wavelength and pump−probe delay, for hybrid fibers embedding NWs. Figure 5b shows $\Delta T/T$ spectra at selected pump−probe delays, whereas Figure 5c,d shows $\Delta T/T$ dynamics at selected probe wavelengths. The corresponding results for fibers embedding NPs, shown in Figure S8, display a similar behavior. The excitation fluence is 250 μJ cm^{-2}, which corresponds to a carrier density of 6.78 × 10^{16} cm^{-3} (see Supporting Information), more than 1 order of magnitude below the threshold for the Mott transition in ZnO.[44] The $\Delta T/T$ spectrum at 1 ps pump−probe delay (Figure 5b) shows a positive signal at 365−380 nm, which is assigned to photobleaching (PB) of the excitonic transition (i.e., reduced absorption of the sample following photoexcitation), as expected on the basis of the absorption spectra reported in Figure 4a. Importantly, a positive $\Delta T/T$ signal is also observed for wavelengths in the 380−400 nm range, which corresponds
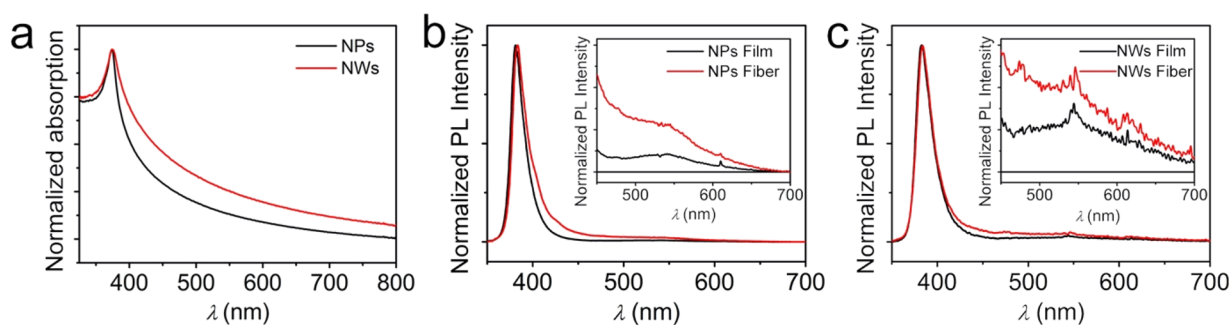

Figure 4. (a) Normalized absorption spectra of PMMA films doped with ZnO NPs (black line) and NWs (red line). (b,c) Normalized PL emission of films (black lines) and fibers (red lines) doped with ZnO NPs (b) and NWs (c). Insets: Magnified PL spectra in the visible spectral range.
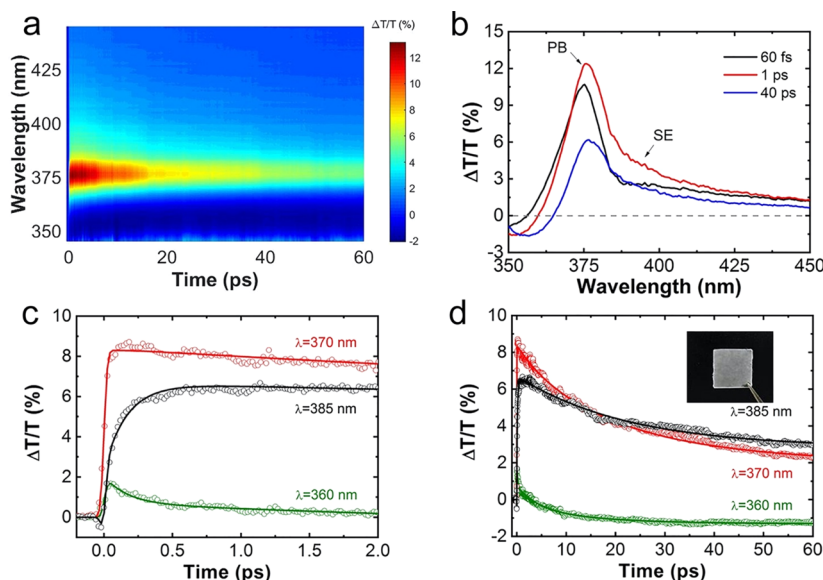
Figure 5. Femtosecond pump−probe spectroscopy of fibers doped with ZnO NWs. (a) 2D $\Delta T/T$ map as a function of probe wavelength and pump−probe delay. (b) $\Delta T/T$ spectra at selected pump−probe delays. (c,d) $\Delta T/T$ dynamics at selected probe wavelengths for short (c) and long (d) delays. Pump−probe measurements are performed on samples from solutions with χ = 10% [see picture in the inset of panel (d)] to avoid overattenuation of transmission and spectral artifacts due to light scattering from the bulk nanocomposite.

to the UV spectral region of the excitonic PL (Figure 4b,c). Such a positive signal can be attributed to stimulated emission (SE), suggesting the presence of net optical gain[45] in the material. Finally, a positive signal is also observed at longer wavelengths, up to 450 nm, and is attributed to a combination of PB and SE arising from ZnO surface states and defects. The $\Delta T/T$ data are subjected to global analysis,[46] and the corresponding decay associated spectra (DAS) are shown in Figure S9. DAS1 has a time constant of ∼240 fs and can be attributed to the relaxation of the photogenerated hot carriers through coupling with optical phonons.[47] DAS1 shows the buildup of the SE band peaking at 380 nm (as confirmed by the 385 nm dynamics in Figure 5c) as well as the buildup of a photoinduced absorption (PA) band peaking at 360 nm. This PA band[48,49] can be tentatively assigned to the Burstein−Moss effect. DAS2, with a weak amplitude and a 5.6 ps time constant, may be attributed to further carrier thermalization via equilibration of optical and acoustic phonons. DAS3 corresponds to a decay of the PB and SE signals and has a time constant of 38.7 ps, in good agreement with previous time-resolved PL studies of ZnO,[50,51] which attributed it to the decay of free excitons. Finally, the long-lived DAS4 corresponds to the decay of excitons bound to defects and band-edge states. Overall, the ultrafast studies clearly suggest that the hybrid fibers with both NPs and NWs can be a promising flexible gain media for UV lasing.

To demonstrate the use of these systems in mirrorless laser sources, ASE measurements are carried out by optically pumping uniaxially aligned arrays of fibers with long-pulse (ns) excitation at λ = 355 nm. The pump light is polarized parallel to the fiber length and shaped as a stripe with a size of 10×0.2 mm^2, which is aligned parallel to fibers. ASE is generated by the amplification of spontaneously emitted photons by SE under intense optical excitation,[52] a process that can be also assisted by the waveguiding of light along the polymer fibers with ZnO NWs. ASE displays a characteristic spectral line-narrowing upon increasing the excitation intensity. Such line-narrowing occurs in the spectral region of the

maximum net gain of the active material, which is related to the SE cross-section and to the spontaneous emission rate of the active material as well as to the propagation losses and the properties of light modes in the waveguide. No ASE is found in hybrid filaments doped with ZnO NPs, evidencing the critically important role of waveguiding in assisting ASE along polymer matrices and nanocomposites. Indeed, upon NP-doping, the rough fiber surface (Figure 2e) disfavors efficient waveguiding and consequently amplification of light emitted by ZnO. Rayleigh scattering from surface defects is likely to be a significant source of optical losses, whose magnitude coefficient per unit propagation length (α) can be estimated by using a formulation of the Rayleigh criterion originally derived for slab waveguides:[53]

$$\alpha = (4\pi/\lambda_{ASE})^2 \times (\cos^3\theta_i/2\sin\theta_i) \times [R_q{}^2/(D + L)] \quad (1)$$

In eq 1, θ_i indicates the angle of incidence, on the fiber surface, of the optical mode propagating along the waveguide with wavelength λ_{ASE} (for PMMA waveguides, one has $\theta_i > 75°$), D is the fiber diameter, and L is the mode penetration depth into the environment surrounding the fiber ($L \ll D$ for D of the order of micrometers). This leads to an optical loss coefficient associated with surface Rayleigh scattering from ZnO NP-doped fibers about five times larger than the corresponding value for NW-in-fibers, which may explain the lack of ASE in the system embedding nonelongated ZnO NPs.

Figure 6 shows the ASE spectra that are instead obtained by ZnO NW-in-fibers, at various pump fluences and the corresponding light−light (L−L) plot. The typical spontaneous emission of ZnO NWs, with a spectrum peaking at about 384 nm, can be observed at low excitation fluence (≤500 μJ cm^{-2}) in Figure 6a. Upon increasing the excitation fluence above about 600 μJ cm^{-2}, a sharp peak at about 382 nm is initially observed, which very rapidly increases in intensity as is typical of ASE (circles in Figure 6b). In fact, due to the multiple mechanisms at play, the peak wavelength of ASE does not coincide with the peak wavelength of the spontaneous
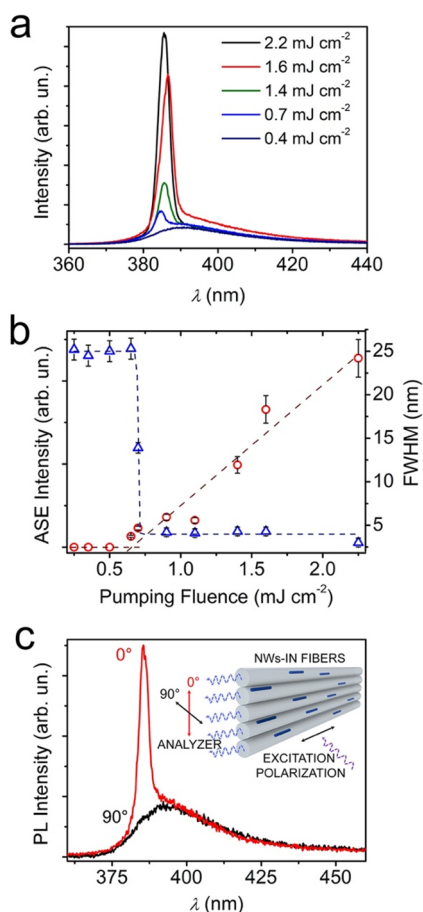
Figure 6. (a) PL spectra of NW-in-fibers for different pump fluences, highlighting the ASE peak. (b) ASE intensity (red circles, left vertical scale) and FWHM of the spectra (blue triangles, right vertical scale) as a function of the pump fluence. (c) Polarization-dependent ASE intensity from NW-in-fibers. The emitted light is collected from the cut end of the fibers by an analyzer with polarization parallel (0°, red line) and perpendicular (90°, black line) to the sample surface (scheme in the inset). χ = 30%.

systems based on ZnO nanomaterials such as polydimethylsiloxane nanocomposite films and zinc oxide-silica systems (generally in the range 2−4 mJ cm^{-2}).[57,58] Various effects might contribute in enhancing ASE features in UV light-emitting fibers with respect to films, such as the alignment of ZnO NWs along the fiber length which leads to more effective photoexcitation as well as waveguiding along the longitudinal axis of the aligned filaments which directly promotes ASE.[59]

In addition, ASE from NW-in-fibers is found to be polarized along the direction parallel to the sample surface ("0°" curve in Figure 6c). This can be explained by the higher propagation losses experienced by light with polarization component perpendicular to the sample surface ("90°" curve in Figure 6c), due to more intense outcoupling into the quartz substrate underneath.[60,61] The linearly polarized ASE could be exploited for significantly improving the signal-to-noise ratio in diagnostic chips working through fluorescence excitation.[62] To this aim, also noteworthy is the high directionality of the emitted light. We analyze the ASE beam profile of aligned NW-in-fibers at various distances from the tip (Figure 7a),
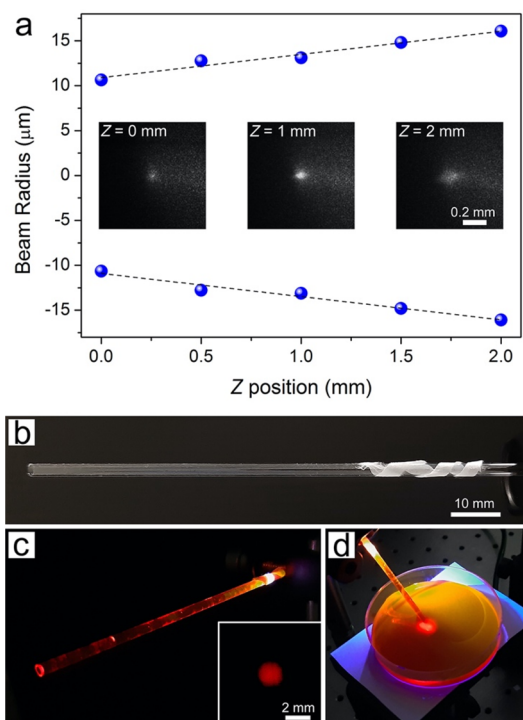

Figure 7. (a) Measured ASE beam divergence. ASE beam radius (dots) vs detector distance, Z. Inset: Micrographs of the emission spot measured at different distances. (b−d) Examples of hybrid NW-in-fibers coupled with nonplanar surfaces and optical systems. (b) NW-in-fiber mat wrapped around the curved surface of a capillary glass tube. (c,d) The UV light from NW-in-fibers excites a viscous Rhodamine 6G solution in the tube. The light emitted by the dye is then guided along glass and the viscous fluid and generates a ∼2 mm spot (inset of panel c) at the capillary end for liquid sample illumination (d).

emission. In particular, the ASE peak is found to correspond to the spectral region of excitonic recombination, while ZnO surface states and defects contributing to the broader spontaneous emission do not appear to undergo SE assisted by waveguiding in the electrospun polymer fibers. We also find a blueshift (9 meV) of the ASE peak energy for very high excitation fluences (from 1.6 up to 2.2 mJ cm^{-2}), which is a signature of the increasing screening of the exciton binding energy, as a consequence of the increased density of electron−hole pairs created upon photoexcitation.[54,55] Such effect competes with the band gap renormalization that typically red shifts the gain profile as the excitation intensity is increased,[54] as here found for excitation fluences up to 1.6 mJ cm^{-2}. Correspondingly, the full width at half-maximum (FWHM) of the PL spectrum decreases from 25 nm to about 4 nm (triangles in Figure 6b) upon increasing the excitation fluence. Although ASE is an inherently thresholdless phenomenon,[56] an experimental effective threshold is usually introduced to quantitatively describe gain narrowing, defined as the halfway fluence between the spontaneous emission and the narrowed ASE line width regimes. Here we measure a threshold of 650 μJ cm^{-2} for ZnO NW-in-fibers that is significantly lower than values reported for other hybrid

evidencing a divergence of 5 mrad, which is lower than that reported for other polymer light-emitting systems in the form of film[63] or fibers[3] (Table S1). Data for ZnO NW-doped films are displayed in Figure S10. They exhibit a worse ASE performance, with a more than 1 order of magnitude higher

threshold, which we attribute to the disordered internal configuration of the dopants.

Finally, the NW-in-fiber hybrids conform enough to be wrapped around curved surfaces with a mm-scale curvature radius such as capillary glass tubes (Figure 7b), thus adapting to specific excitation schemes (Figure 7c,d). For instance, the UV light emitted by the optically pumped hybrids here in contact with the glass tube is able to excite chromophores (Rhodamine 6G dye) flowing in the capillary (Figure 7c). The light emitted by the dye can then be guided along the same capillary for centimeters, until it generates a well-defined exit spot (inset of Figure 7c) for remote sample illumination at the chromophore wavelength, as shown by a solution in the plate photographed in Figure 7e.

A summary of the emissive properties for ZnO NW-in-fibers is reported in Table S1, comparing achieved performance with those of other miniaturized, optically excited UV light-emitting materials. Overall, the occurrence of ASE under long-pulse pump conditions, combined with the photo- and chemical stability of embedded ZnO nanostructures, the high directionality of the emitted light, and the achieved flexibility of the hybrid material, makes NW-in-fibers excellent and versatile active media for flexible UV lasers that can be coupled with curved optical components or integrated in miniaturized diagnostics and microfluidic devices.

CONCLUSION

In summary, we have introduced light-emitting NW-in-fiber hybrid materials with optical gain in the UV and with a highly favorable combination of properties. We performed an extensive optical characterization of the electrospun fibers. High time-resolution pump−probe spectroscopy in the UV detected stimulated emission in the 380−400 nm wavelength range, while line narrowing in this spectral range provided a signature of ASE, with onset for excitation fluence of 650 μJ cm^{-2}. ASE in the fibers with an internal order of ZnO NWs, leading to more effective optical behavior, features a lower excitation threshold compared to other nanohybrid materials and components based on ZnO nanocrystals. These properties, obtained in flexible and conformable fiber mats, make these materials highly interesting for various applications in sensing and light-emitting devices, bioimaging, and photo-cross-linking as well as in network and bendable microlasers. Upon engineering the strength of the ZnO/polymer interface through proper surface modifiers or cross-linking of the organic matrix, one could also aim to obtain effective strain and load transfer to the inorganic component,[64,65] a perspective highly interesting for opto-mechanical coupling,[66] and to exploit the piezoelectric properties of NWs in the hybrid material.

METHODS

Hybrid NW-in-Fibers. ZnO NWs (manufacture code 773999) and ZnO NPs (manufacture code 544906) with high purity[67−69] were purchased from Sigma-Aldrich. X-ray diffraction (XRD) data on these materials[69−72] indicate typical hexagonal wurtzite structures with high crystallinity. PMMA (average molecular weight ∼120,000 Da), and chloroform were purchased from Sigma-Aldrich. Ethanol was purchased from Fluka, and DMF was purchased from Carlo Erba. Solutions for electrospinning were prepared by 250 mg mL^{-1} of PMMA dissolved in a mix of chloroform, ethanol, and DMF with a volume ratio of 4:4:1 and ZnO NPs or NWs added at a relative weight ratio (χ) between 10% and 50% with respect to the polymer. The solution was loaded in a syringe with a 27 gauge needle and injected through the needle at constant flow rate of 1 mL h^{-1} by a microprocessor dual-drive syringe pump (33 Dual Syringe Pump, Harvard Apparatus Inc., Holliston, MA). A voltage of 12 kV (XRM30P, Gamma High Voltage Research Inc., Ormond Beach, FL) was applied to the spinneret, and fibers were collected at distance of 10 cm from the needle on a metallic collector biased at −6 kV. Either a plate or a rotating collector (disk with 0.8 cm width, 8 cm diameter, 4000 rpm) was used to obtain randomly oriented or aligned fibers, respectively.

Morphological and Optical Characterization. The morphology of the hybrid fibers was investigated by SEM, TEM, and AFM. For SEM analysis, fibers were collected on Si substrates, and images were acquired by a FEI Helios 600i system, operating at acceleration voltages of 3−5 kV. TEM images were acquired with a JEOL JEM 1011 microscope operating at accelerating voltage of 100 kV. For particle inspection, a few drops of dispersions were drop-casted onto 300 mesh carbon-coated grids, and the residual solvent was allowed to evaporate at room temperature. For fibrous samples, 400 mesh copper grids were temporarily fixed on the electrospinning collector by carbon tape, and a few fibers were deposited onto them in a short time lapse (≅10 s) for subsequent imaging. All images were acquired and processed by Gatan Digital Micrograph 2.3 native software. AFM measurements were carried out by a Multimode system equipped with a Nanoscope IIIa electronic controller (Veeco Instruments). The fiber topography was analyzed in tapping mode, utilizing Si cantilevers with 190 kHz resonance frequency and with tips featuring a nominal radius of 8 nm, length in the range 10−15 μm, and apex angle of 22.5°. The width and height of the cross-sectional profile of the NW-in-fiber (Figure 2f), calculated upon deconvolution with the profile of the used AFM tip, are indicative of an almost circular cross-section (∼1 and ∼0.9 μm, respectively).

Fluorescence and transmitted light micrographs were collected by means of an inverted microscope Eclipse Ti (Nikon), using a 20× (numerical aperture, NA = 0.50, Nikon) and a 60× (NA = 1.40, Nikon) objective. Fluorescence images were acquired by exciting samples with a Hg lamp and collecting the emitted light with a digital camera DS-Ri1 (Nikon). Maps of the light transmitted by samples were collected by scanning a focused argon ion laser (λ = 488 nm). Absorption spectra were collected by a double beam UV−vis spectrophotometer (PerkinElmer).

PL, ASE, and Pump−Probe Experiments. PL and ASE measurements were carried out by exciting NW-in-fibers, deposited on quartz substrates, by the third harmonic of a ns Nd:YAG laser (Quanta-Ray INDI Spectra-Physics), with emission wavelength at λ = 355 nm and a repetition rate of 10 Hz. The propagation direction of the incident pumping beam was set perpendicular to the sample surface, and the emission was collected from the sample edge, namely at 90° with respect to the excitation beam, through a fiber-coupled imaging spectrometer (iHR320, Jobin Yvon) equipped with a charge coupled device (Simphony, Jobin Yvon). Beam divergence measurements were performed on aligned fibers excited above threshold. A Si CCD was used to measure the spatial profile of the emitted beam, and the divergence was estimated by plotting the measured beam diameter *vs* the detector position and evaluating the half angle corresponding to the asymptotic variation of the beam radius along the propagation direction.

Femtosecond pump−probe experiments were performed starting from an amplified Ti:sapphire system (Libra, Coherent) generating 4 mJ, 100 fs pulses at 800 nm central wavelength, and 1 kHz repetition rate. A fraction of the laser output was used to pump a noncollinear optical parametric amplifier (NOPA), which generates sub-20 fs visible pulses at 540 nm. Sum-frequency generation of the NOPA output with the 800 nm pulse in a 50 μm-thick type II β-barium borate crystal produced the sub-20 fs pump pulses with spectrum centered at 335 nm.[73] Another fraction of the laser output was focused in a 3 mm-thick CaF$_2$ plate, to generate a white-light continuum covering the 330−650 nm wavelength range, used as broadband probe pulse. Pump and probe pulses, both polarized parallel to the direction of fibers, were noncollinearly focused on the sample, and the transmitted probe was sent to a spectrometer capable

of single-shot detection at the 1 kHz laser repetition rate. For each measurement, the transmittance of the probe pulse was measured with ($T_{\text{pump\_ON}}$) and without ($T_{\text{pump\_OFF}}$) a preceding excitation pulse. The relative changes in transmittance are expressed as $\Delta T/T$ (%) = $[(T_{\text{pump\_ON}} - T_{\text{pump\_OFF}})/T_{\text{pump\_OFF}}] \times 100$. A detailed description of the femtosecond pump−probe system can be found in ref 74. Global analysis of the pump−probe data was performed using the Glotaran software obtaining the DAS and the corresponding time constants.[75]

ASSOCIATED CONTENT

Ⓢ Supporting Information

The Supporting Information is available free of charge at https://pubs.acs.org/doi/10.1021/acsnano.0c00870.

Additional details and calculations on ZnO NPs solubility, diameter distribution of hybrid fibers, TEM analysis, and estimation of the ZnO/PMMA volumetric ratio, calculated waveguiding and scattering properties, PL and ASE emission, estimation method for the photoexcited carrier density, femtosecond pump−probe spectroscopy of fibers with ZnO NPs, decay associated spectra, and ASE spectra of NW-doped films (PDF)

AUTHOR INFORMATION

Corresponding Authors

Giulio Cerullo − *IFN-CNR, Dipartimento di Fisica, Politecnico di Milano, I-20133 Milano, Italy;* ⓞ orcid.org/0000-0002-9534-2702; Email: giulio.cerullo@polimi.it

Dario Pisignano − *NEST, Istituto Nanoscienze-CNR, I-56127 Pisa, Italy; Dipartimento di Fisica, Università di Pisa, I-56127 Pisa, Italy;* ⓞ orcid.org/0000-0003-3758-5199; Email: dario.pisignano@unipi.it

Authors

Alberto Portone − *NEST, Istituto Nanoscienze-CNR, I-56127 Pisa, Italy; NEST, Scuola Normale Superiore, I-56127 Pisa, Italy; Dipartimento di Matematica e Fisica "Ennio De Giorgi", Università del Salento, I-73100 Lecce, Italy*

Rocio Borrego-Varillas − *IFN-CNR, Dipartimento di Fisica, Politecnico di Milano, I-20133 Milano, Italy*

Lucia Ganzer − *IFN-CNR, Dipartimento di Fisica, Politecnico di Milano, I-20133 Milano, Italy*

Riccardo Di Corato − *Institute for Microelectronics and Microsystems, CNR-IMM, Campus Ecotekne, I-73100 Lecce, Italy;* ⓞ orcid.org/0000-0002-7173-6176

Antonio Qualtieri − *Center for Biomolecular Nanotechnologies, Istituto Italiano di Tecnologia, I-73010 Arnesano,, Italy*

Luana Persano − *NEST, Istituto Nanoscienze-CNR, I-56127 Pisa, Italy; NEST, Scuola Normale Superiore, I-56127 Pisa, Italy*

Andrea Camposeo − *NEST, Istituto Nanoscienze-CNR, I-56127 Pisa, Italy; NEST, Scuola Normale Superiore, I-56127 Pisa, Italy*

Complete contact information is available at:
https://pubs.acs.org/10.1021/acsnano.0c00870

Notes

The authors declare no competing financial interest.

REFERENCES

(1) Schneider, D.; Rabe, T.; Riedl, T.; Dobbertin, T.; Kröger, M.; Becker, E.; Johannes, H.-H.; Kowalsky, W.; Weimann, T.; Wang, J.; Hinze, P.; Gerhard, A.; Stossel, P.; Vestweber, H. An Ultraviolet Organic Thin-Film Solid-State Laser for Biomarker Applications. *Adv. Mater.* **2005**, *17*, 31−34.

(2) Vladisavljević, G. T.; Khalid, N.; Neves, M. A.; Kuroiwa, T.; Nakajima, M.; Uemura, K.; Ichikawa, S.; Kobayashi, I. Industrial Lab-On-A-Chip: Design, Applications and Scale-Up for Drug Discovery and Delivery. *Adv. Drug Delivery Rev.* **2013**, *65*, 1626−1663.

(3) Morello, G.; Manco, R.; Moffa, M.; Persano, L.; Camposeo, A.; Pisignano, D. Multifunctional Polymer Nanofibers: UV Emission, Optical Gain, Anisotropic Wetting, and High Hydrophobicity for Next Flexible Excitation Sources. *ACS Appl. Mater. Interfaces* **2015**, *7*, 21907−21912.

(4) Cai, P.; Huang, Y.; Seo, H. J. Anti-Stokes Ultraviolet Luminescence and Exciton Detrapping in the Two-Dimensional Perovskite $(C_6H_5C_2H_4NH_3)_2PbCl_4$. *J. Phys. Chem. Lett.* **2019**, *10*, 4095−4102.

(5) Yang, W.; Zhang, Y.; Zhang, Y.; Deng, W.; Fang, X. Transparent Schottky Photodiode Based on AgNi NWs/SrTiO$_3$ Contact with an Ultrafast Photoresponse to Short-Wavelength Blue Light and UV-Shielding Effect. *Adv. Funct. Mater.* **2019**, *29*, 1905923.

(6) Wang, M.; Wang, C.; Chen, M.; Xi, Y.; Cheng, W.; Mao, C.; Xu, T.; Zhang, X.; Lin, C.; Gao, W.; Guo, Y.; Lei, B. Efficient Angiogenesis-Based Diabetic Wound Healing/Skin Reconstruction through Bioactive Antibacterial Adhesive Ultraviolet Shielding Nanodressing with Exosome Release. *ACS Nano* **2019**, *13*, 10279−10293.

(7) Huang, M. H.; Mao, S.; Feick, H.; Yan, H.; Wu, Y.; Kind, H.; Weber, E.; Russo, R.; Yang, P. Room-Temperature Ultraviolet Nanowire Nanolasers. *Science* **2001**, *292*, 1897−1899.

(8) Johnson, J. C.; Choi, H. J.; Knutsen, K. P.; Schaller, R. D.; Yang, P.; Saykally, R. J. Single Gallium Nitride Nanowire Lasers. *Nat. Mater.* **2002**, *1*, 106−110.

(9) Pauzauskie, P. J.; Sirbuly, D. J.; Yang, P. Semiconductor Nanowire Ring Resonator Laser. *Phys. Rev. Lett.* **2006**, *96*, 143903.

(10) Zhou, H.; Wissinger, M.; Fallert, J.; Hauschild, R.; Stelzl, F.; Klingshirn, C.; Kalt, H. Ordered Uniform-Sized ZnO Nanolaser Arrays. *Appl. Phys. Lett.* **2007**, *91*, 181112.

(11) Liu, H.; Hu, L.; Watanabe, K.; Hu, X.; Dierre, B.; Kim, B.; Sekiguchi, T.; Fang, X. Cathodoluminescence Modulation of ZnS Nanostructures by Morphology, Doping, and Temperature. *Adv. Funct. Mater.* **2013**, *23*, 3701−3709.

(12) Zhang, Q.; Li, G.; Liu, X.; Qian, F.; Li, Y.; Sum, T. C.; Lieber, C. M.; Xiong, Q. A. A Room Temperature Low-Threshold Ultraviolet Plasmonic Nanolaser. *Nat. Commun.* **2014**, *5*, 4953.

(13) Yang, W.; Hu, K.; Teng, F.; Weng, J.; Zhang, Y.; Fang, X. High-Performance Silicon-Compatible Large-Area UV-To-Visible Broadband Photodetector Based on Integrated Lattice-Matched Type II Se/n-Si Heterojunctions. *Nano Lett.* **2018**, *18*, 4697−4703.

(14) Qiu, C. F.; Wang, L. D.; Chen, H. Y.; Wong, M.; Kwok, H. S. Room-Temperature Ultraviolet Emission from an Organic Light-Emitting Diode. *Appl. Phys. Lett.* **2001**, *79*, 2276−2278.

(15) Spehr, T.; Siebert, A.; Fuhrmann-Lieker, T.; Salbeck, J.; Rabe, T.; Riedl, T.; Johannes, H. H.; Kowalsky, W.; Wang, J.; Weimann, T.; Hinze, P. Organic Solid-State Ultraviolet-Laser Based on Spiro-Terphenyl. *Appl. Phys. Lett.* **2005**, *87*, 161103.

(16) Zhao, Y. S.; Peng, A.; Fu, H.; Ma, Y.; Yao, J. Nanowire Waveguides and Ultraviolet Lasers Based on Small Organic Molecules. *Adv. Mater.* **2008**, *20*, 1661−1665.

(17) Forget, S.; Rabbani-Haghighi, H.; Diffalah, N.; Siove, A.; Chénais, S. Tunable Ultraviolet Vertically-Emitting Organic Laser. *Appl. Phys. Lett.* **2011**, *98*, 131102.

(18) Gaio, M.; Moffa, M.; Castro-Lopez, M.; Pisignano, D.; Camposeo, A.; Sapienza, R. Modal Coupling of Single Photon Emitters within Nanofiber Waveguides. *ACS Nano* **2016**, *10*, 6125−6130.

(19) Little, A.; Hoffman, A.; Haegel, N. M. Optical Attenuation Coefficient in Individual ZnO Nanowires. *Opt. Express* **2013**, *21*, 6321−6326.

(20) Zhang, J.; Wen, B.; Wang, F.; Ding, Y.; Zhang, S.; Yang, M. *In Situ* Synthesis of ZnO Nanocrystal/PET Hybrid Nanofibers *via* Electrospinning. *J. Polym. Sci., Part B: Polym. Phys.* **2011**, *49*, 1360−1368.

(21) Ortac, B.; Kayaci, F.; Vural, H. A.; Deniz, A. E.; Uyar, T. Photoluminescent Electrospun Polymeric Nanofibers Incorporating Germanium Nanocrystals. *React. Funct. Polym.* **2013**, *73*, 1262−1267.

(22) Teke, A.; Ozgur, U.; Dogan, S.; Gu, X.; Morkoc, H.; Nemeth, B.; Nause, J.; Everitt, H. O. Excitonic Fine Structure and Recombination Dynamics in Single-Crystalline ZnO. *Phys. Rev. B: Condens. Matter Mater. Phys.* **2004**, *70*, 195207.

(23) Tsukazaki, A.; Ohtomo, A.; Onuma, T.; Ohtani, M.; Makino, T.; Sumiya, M.; et al. Repeated Temperature Modulation Epitaxy for *p*-Type Doping and Light-Emitting Diode Based on ZnO. *Nat. Mater.* **2005**, *4*, 42−46.

(24) Fang, X.; Bando, Y.; Gautam, U. K.; Zhai, T.; Zeng, H.; Xu, X.; Liao, M.; Golberg, D. ZnO and ZnS Nanostructures: Ultraviolet-Light Emitters, Lasers, and Sensors. *Crit. Rev. Solid State Mater. Sci.* **2009**, *34*, 190−223.

(25) Lai, Y. Y.; Lan, Y. P.; Lu, T. C. Strong Light−Matter Interaction in ZnO Microcavities. *Light: Sci. Appl.* **2013**, *2*, No. e76.

(26) Bashouti, M.; Salalha, W.; Brumer, M.; Zussman, E.; Lifshitz, E. Alignment of Colloidal CdS Nanowires Embedded in Polymer Nanofibers by Electrospinning. *ChemPhysChem* **2006**, *7*, 102−106.

(27) Terekhov, P. D.; Baryshnikova, K. V.; Shalin, A. S.; Karabchevsky, A.; Evlyukhin, A. B. Resonant Forward Scattering of Light by High-Refractive-Index Dielectric Nanoparticles with Toroidal Dipole Contribution. *Opt. Lett.* **2017**, *42*, 835.

(28) Mangalgiri, G. M.; Manley, P.; Riedel, W.; Schmid, M. Dielectric Nanorod Scattering and Its Influence on Material Interfaces. *Sci. Rep.* **2017**, *7*, 4311.

(29) Vogt, K. E.; Gerharz, S.; Graham, J.; Canepari, M. High-Resolution Simultaneous Voltage and Ca^{2+} Imaging. *J. Physiol.* **2011**, *589*, 489−494.

(30) Pathak, G. P.; Vrana, J. D.; Tucker, C. L. Optogenetic Control of Cell Function Using Engineered Photoreceptors. *Biol. Cell* **2013**, *105*, 59−72.

(31) Guan, N.; Dai, X.; Babichev, A. V.; Julien, F. H.; Tchernycheva, M. Flexible Inorganic Light Emitting Diodes Based on Semiconductor Nanowires. *Chem. Sci.* **2017**, *8*, 7904−7911.

(32) Yun, S. H.; Kwok, S. J. Light in Diagnosis, Therapy and Surgery. *Nat. Biomed. Eng.* **2017**, *1*, 0008.

(33) Yousefi, R.; Kamaluddin, B. Dependence of Photoluminescence Peaks and ZnO Nanowires Diameter Grown on Silicon Substrates at Different Temperatures and Orientations. *J. Alloys Compd.* **2009**, *479*, L11−L14.

(34) Yang, P.; Yan, H.; Mao, S.; Russo, R.; Johnson, J.; Saykally, R.; Morris, N.; Pham, J.; He, R.; Choi, H. J. Controlled Growth of ZnO Nanowires and Their Optical Properties. *Adv. Funct. Mater.* **2002**, *12*, 323−331.

(35) Senger, R.; Bajaj, K. Optical Properties of Confined Polaronic Excitons in Spherical Ionic Quantum Dots. *Phys. Rev. B: Condens. Matter Mater. Phys.* **2003**, *68*, No. 045313.

(36) Felbier, P.; Yang, J.; Theis, J.; Liptak, R. W.; Wagner, A.; Lorke, A.; Bacher, G.; Kortshagen, U. Highly Luminescent ZnO Quantum Dots Made in a Nonthermal Plasma. *Adv. Funct. Mater.* **2014**, *24*, 1988−1993.

(37) Di Benedetto, F.; Camposeo, A.; Persano, L.; Laera, A. M.; Piscopiello, E.; Cingolani, R.; Tapfer, L.; Pisignano, D. Light-Emitting Nanocomposite CdS−Polymer Electrospun Fibres *via In Situ* Nanoparticle Generation. *Nanoscale* **2011**, *3*, 4234−4239.

(38) O'Carroll, D.; Lieberwirth, I.; Redmond, G. Microcavity Effects and Optically Pumped Lasing in Single Conjugated Polymer Nanowires. *Nat. Nanotechnol.* **2007**, *2*, 180−184.

(39) Dror, Y.; Salalha, W.; Khalfin, R. L.; Cohen, Y.; Yarin, A. L.; Zussman, E. Carbon Nanotubes Embedded in Oriented Polymer Nanofibers by Electrospinning. *Langmuir* **2003**, *19*, 7012−7020.

(40) Segets, D.; Gradl, J.; Taylor, R. K.; Vassilev, V.; Peukert, W. Analysis of Optical Absorbance Spectra for the Determination of ZnO Nanoparticle Size Distribution, Solubility, and Surface Energy. *ACS Nano* **2009**, *3*, 1703−1710.

(41) Ozgur, U.; Alivov, Y. I.; Liu, C.; Teke, A.; Reshchikov, M. A.; Dogan, S.; Avrutin, V.; Cho, S.-J.; Morkoc, H. A Comprehensive Review of ZnO Materials and Devices. *J. Appl. Phys.* **2005**, *98*, No. 041301.

(42) Johnston, K.; Henry, M. O.; McCabe, D.; McGlynn, E.; Dietrich, M.; Alves, E.; Xia, M. Identification of Donor-Related Impurities in ZnO Using Photoluminescence and Radiotracer Techniques. *Phys. Rev. B: Condens. Matter Mater. Phys.* **2006**, *73*, 165212.

(43) Zhang, L.; Yin, L.; Wang, C.; Lun, N.; Qi, Y.; Xiang, D. Origin of Visible Photoluminescence of ZnO Quantum Dots: Defect-Dependent and Size-Dependent. *J. Phys. Chem. C* **2010**, *114*, 9651−9658.

(44) Versteegh, M. A. M.; Kuis, T.; Stoof, H. T. C.; Dijkhuis, J. I. Ultrafast Screening and Carrier Dynamics in ZnO: Theory and Experiment. *Phys. Rev. B: Condens. Matter Mater. Phys.* **2011**, *84*, No. 035207.

(45) Appavoo, K.; Liu, X.; Menon, V.; Sfeir, M. Y. Excitonic Lasing in Solution-Processed Subwavelength Nanosphere Assemblies. *Nano Lett.* **2016**, *16*, 2004−2010.

(46) van Stokkum, I. H. M.; Larsen, D. S.; van Grondelle, R. Global and Target Analysis of Time-Resolved Spectra. *Biochim. Biophys. Acta, Bioenerg.* **2004**, *1657*, 82−104.

(47) Bernardi, M.; Vigil-Fowler, D.; Ong, C. S.; Neaton, J. B.; Louie, S. G. *Ab Initio* Study of Hot Electrons in GaAs. *Proc. Natl. Acad. Sci. U. S. A.* **2015**, *112*, 5291−5296.

(48) Yamamoto, A.; Kido, T.; Goto, T.; Chen, Y.; Yao, T.; Kasuya, A. Dynamics of Photoexcited Carriers in ZnO Epitaxial Thin Films. *Appl. Phys. Lett.* **1999**, *75*, 469−471.

(49) Sun, C.-K.; Sun, S.-Z.; Lin, K.-H.; Zhang, K. Y.-J.; Liu, H.-L.; Liu, S.-C.; Wu, J.-J. Ultrafast Carrier Dynamics in ZnO Nanorods. *Appl. Phys. Lett.* **2005**, *87*, No. 023106.

(50) Guo, B.; Ye, Z.; Wong, K. S. Time-Resolved Photoluminescence Study of a ZnO Thin Film Grown on a (1 0 0) Silicon Substrate. *J. Cryst. Growth* **2003**, *253*, 252−257.

(51) Johnson, J. C.; Knutsen, K. P.; Yan, H.; Law, M.; Zhang, Y.; Yang, P.; Saykally, R. J. Ultrafast Carrier Dynamics in Single ZnO Nanowire and Nanoribbon Lasers. *Nano Lett.* **2004**, *4*, 197−204.

(52) Svelto, O.; Taccheo, S.; Svelto, C. Analysis of Amplified Spontaneous Emission: Some Corrections to the Linford Formula. *Opt. Commun.* **1998**, *149*, 277−282.

(53) Tien, P. K. Light Waves in Thin Films and Integrated Optics. *Appl. Opt.* **1971**, *10*, 2395−2413.

(54) Johnson, J. C.; Yan, H.; Yang, P.; Saykally, R. J. Optical Cavity Effects in ZnO Nanowire Lasers and Waveguides. *J. Phys. Chem. B* **2003**, *107*, 8816−8828.

(55) Empizo, M. J. F.; Yamanoi, K.; Santos-Putungan, A. B.; Arita, R.; Minami, Y.; Luong, M. V.; Shimizu, T.; Estacio, E. S.; Somintac, A. S.; Salvador, A. A.; Sarmago, R. V.; Sarukura, N. Blue-Shifted and Picosecond Amplified UV Emission from Aqueous Chemical Grown ZnO Microrods. *Opt. Mater.* **2015**, *48*, 179−184.

(56) Svelto, O. *Principles of Lasers*, 5th ed.; Plenum Press: New York, 1989; pp 71−76.

(57) Anglos, D.; Stassinopoulos, A.; Das, R. N.; Zacharakis, G.; Psyllaki, M.; Jakubiak, R.; Vaia, R. A.; Giannelis, E. P.; Anastasiadis, S. H. Random Laser Action in Organic−Inorganic Nanocomposites. *J. Opt. Soc. Am. B* **2004**, *21*, 208−213.

(58) Stassinopoulos, A.; Das, R. N.; Anastasiadis, S. H.; Giannelis, E. P.; Anglos, D. Random Lasing Action from ZnO−Silica Nanohybrids. *J. Opt.* **2010**, *12*, No. 024006.

(59) Morello, G.; Moffa, M.; Girardo, S.; Camposeo, A.; Pisignano, D. Optical Gain in the Near Infrared by Light-Emitting Electrospun Fibers. *Adv. Funct. Mater.* **2014**, *24*, 5225−5231.

(60) Li, H. Y.; Ruhle, S.; Khedoe, R.; Koenderink, A. F.; Vanmaekelbergh, D. Polarization, Microscopic Origin, and Mode Structure of Luminescence and Lasing from Single ZnO Nanowires. *Nano Lett.* **2009**, *9*, 3515−3520.

(61) Han, N. S.; Shim, H. S.; Lee, S.; Park, S. M.; Choi, M. Y.; Song, J. K. Light−Matter Interaction and Polarization of Single ZnO Nanowire Lasers. *Phys. Chem. Chem. Phys.* **2012**, *14*, 10556−10563.

(62) Pagliara, S.; Camposeo, A.; Polini, A.; Cingolani, R.; Pisignano, D. Electrospun Light-Emitting Nanofibers As Excitation Source in Microfluidic Devices. *Lab Chip* **2009**, *9*, 2851−2856.

(63) Costela, A.; García, O.; Cerdán, L.; García-Moreno, I.; Sastre, R. Amplified Spontaneous Emission and Optical Gain Measurements from Pyrromethene 567-Doped Polymer Waveguides and Quasi-Waveguides. *Opt. Express* **2008**, *16*, 7023−7036.

(64) Grinberg, O.; Deng, S.; Zussman, E.; Livneh, T.; Zak, A. Raman Scattering from Single WS$_2$ Nanotubes in Stretched PVDF Electrospun Fibers. *Phys. Chem. Chem. Phys.* **2017**, *19*, 18443−18451.

(65) Deng, S.; Arinstein, A.; Zussman, E. Size-Dependent Mechanical Properties of Glassy Polymer Nanofibers *via* Molecular Dynamics Simulations. *J. Polym. Sci., Part B: Polym. Phys.* **2017**, *55*, 506−514.

(66) Vazinishayan, A.; Lambada, D. R.; Yang, S.; Zhang, G.; Cheng, B.; Woldu, Y. T.; Shafique, S.; Wang, Y.; Anastase, N. Effects of Mechanical Strain on Optical Properties of ZnO Nanowire. *AIP Adv.* **2018**, *8*, No. 025306.

(67) Dhas, S. P.; Shiny, P. J.; Khan, S.; Mukherjee, A.; Chandrasekaran, N. Toxic Behavior of Silver and Zinc Oxide Nanoparticles on Environmental Microorganisms. *J. Basic Microbiol.* **2014**, *54*, 916−927.

(68) Schiavo, S.; Oliviero, M.; Li, J.; Manzo, S. Testing ZnO Nanoparticle Ecotoxicity: Linking Time Variable Exposure to Effects on Different Marine Model Organisms. *Environ. Sci. Pollut. Res.* **2018**, *25*, 4871−4880.

(69) Yadav, V. K. S.; Daniel, T. T.; Paily, R. Gas Sensors Based on Drop-Casted ZnO Nanowires and Micro-Cantilever Printed Ag Contacts. *IEEE Sens. J.* **2020**, *20*, 4951−4958.

(70) Giusti, G.; Consonni, V.; Puyoo, E.; Bellet, D. High Performance ZnO-SnO$_2$:F Nanocomposite Transparent Electrodes for Energy Applications. *ACS Appl. Mater. Interfaces* **2014**, *6*, 14096−14107.

(71) Louiza, A.; Saliha, H.; Sofiane, H.; Kamel, G.; Lakhder, G. Structural and Luminescence Properties of Pure and Al-Doped ZnO Nanopowders. *Mater. Sci. Eng., B* **2012**, *177*, 902−907.

(72) Zhang, J.; Sun, L.; Pan, H.; Liao, C.; Yan, C. ZnO Nanowires Fabricated by a Convenient Route. *New J. Chem.* **2002**, *26*, 33−34.

(73) Borrego-Varillas, R.; Candeo, A.; Viola, D.; Garavelli, M.; De Silvestri, S.; Cerullo, G.; Manzoni, C. Microjoule-Level, Tunable Sub-10 Fs UV Pulses by Broadband Sum-Frequency Generation. *Opt. Lett.* **2014**, *39*, 3849−3852.

(74) Borrego-Varillas, R.; Ganzer, L.; Cerullo, G.; Manzoni, C. Ultraviolet Transient Absorption Spectrometer with Sub-20-Fs Time Resolution. *Appl. Sci.* **2018**, *8*, 989.

(75) Snellenburg, J. J.; Laptenok, S. P.; Seger, R.; Mullen, K. M.; van Stokkum, I. H. M. Glotaran: A Java-Based Graphical User Interface for the R Package TIMP. *J. Stat. Softw.* **2012**, *49*, 3.